37th AIAA Fluid Dynamics Conference and Exhibit
25 - 28 June 2007, Miami, FL

AIAA 2007-3984

Numerical Simulations of Supersonic Flow in a Linear Aerospike Micronozzle

A. Zilić* D.L. Hitt* A.A. Alexeenko†

* School of Engineering, University of Vermont

† School of Aeronautics & Astronautics, Purdue University

In this study, we numerically examine thrust performance of the linear aerospike nozzle micro-thruster for various nozzle spike lengths and flow parameters in order to identify optimal geometry(s) and operating conditions. Decomposed hydrogen-peroxide is used as the monopropellant in the studies. Performance is characterized for different flow rates (Reynolds numbers) and aerospike lengths, and the impact of micro-scale viscous forces is assessed. It is found that 2-D full micro-aerospike efficiencies can exceed axisymmetric micro-nozzle efficiencies by as much as 10%; however, severe penalties are found to occur for truncated spikes at low Reynolds numbers.

I. Introduction

In recent years significant research has been conducted in the area of micropropulsion systems for orbital maneuvering of next-generation miniaturized satellites ('micro-', 'nano-' and 'pico-sats') having masses ∼10 kg or less. A key component of any chemical-based micropropulsion scheme is the supersonic nozzle used for converting pressure energy of the combustion gases into thrust. In the aerospace literature it has been documented that the flow in supersonic micro-nozzles can be substantially affected by viscous effects, thus reducing the performance of the thruster.[1−6] For the various linear micro-scale nozzles reported in the literature the Reynolds numbers are typically quite low: typical values are well below 1,000 and some less than 500. Consequently, viscous subsonic 'boundary layers' form on the expander wall section which can become sufficiently thick so as to retard the bulk flow and lower the efficiency.

The focus of the present study is a computational investigation of the performance of a 2-D micro-scale *linear aerospike* nozzle design. To the best of our knowledge, this represents the first such report in the aerospace literature. For micropropulsion applications, there is little need for the defining pressure-compensation attribute of the aerospike since the ambient conditions are those of either space or near-space. However, one can seek to leverage the fact that a virtual (free) boundary can potentially *mitigate viscous losses* known to occur for internal micronozzle flows with multiple solid boundaries. This micro-nozzle concept is also worthwhile of investigation owing to its amenability to existing micro-fabrication techniques, a trait not shared by axisymmetric nozzles on the micro-scale.

In this paper, we numerically investigate the thrust production and efficiency of full-length aerospike as well as 20% and 40% truncated geometries ('plug' nozzles) for a range of Reynolds numbers ($< 10^3$) based on estimated mass flow rates for targeted nanosat thrust levels. The working gas is chosen to be a fully-decomposed, 85% hydrogen-peroxide monopropellant. The joint consideration of truncated spikes is based on the prevalence of plug designs in macro-scale nozzles. The latter is often driven by a thrust-to-weight analysis – it has been experimentally observed that the majority of thrust for a macro-scale linear aerospike is generated over the first quarter of the spike. On the micro-scale, the weight savings of a spike truncation is negligible; however, spike truncation instead carries with it implications for boundary layer growth and possible flow separation. It is found that micro-scale aerospikes offer an attractive alternative in performance compared to 3D linear micro-nozzles.

II. Computational Model

A. Numerical Methods for Continuum Flows

H_2O_2 Monopropellant. In this work, the continuum-based flow analyses are focused on the performance of micronozzle flows featuring decomposed monopropellant hydrogen-peroxide originally proposed by Hitt et al.[7] The complete decomposition of the monopropellant fuel is assumed to have occurred upstream of the nozzle within the catalytic chamber. The decomposition of the hydrogen peroxide monopropellant proceeds according to the one-step reaction

$$2H_2O_2(l) \rightarrow 2H_2O(g) + O_2(g) + heat. \tag{1}$$

In the numerical simulations, the thermophysical properties of the gas mixture are assumed to be temperature-dependent and are calculated as a mass-weighted average of the mixture components. The inlet temperature is equal to the fully decomposed adiabatic flame temperature of 85% concentration H_2O_2 and is set at $886\,K$ and serves as an inlet condition to the nozzle. The corresponding Reynolds number for the flow is

$$Re = \frac{\dot{m}L}{\mu A} \tag{2}$$

where $\dot{m}$ is the mass flow rate per unit depth, L is the characteristic length scale (e.g., the nozzle throat diameter), μ is the dynamic viscosity of the decomposed monopropellant, and A is the cross-sectional area. The value of $\dot{m}$ can be well estimated from quasi-1D theory according to[8]

$$\dot{m} = \frac{p_0 A^*}{\sqrt{T_0}} \sqrt{\frac{\gamma}{R}\left(\frac{2}{\gamma+1}\right)^{(\gamma+1)/(\gamma-1)}} \tag{3}$$

where A^* is the nozzle throat area, γ is the ratio of the specifc heats, and R is the gas constant.

Aerospike Geometry & Computational Domain. The idealized spike geometry can be generated using the approach of Angelino.[9] In short, this inviscid approach combines Prandtl-Meyer expansion theory with the area-Mach relation for quasi-1D nozzle flow and determines the spike boundary as a particular streamline in the flow downstream of the nozzle throat. The resulting spike geometry is shown in Figure 1. The length of the nozzles spike is the only varying geometric parameter; here we considered a full length spike, as well as 20% and 40% truncations. A schematic of the entire computational domain is shown in Figure 2. The throat dimension is identical for every micro-nozzle in this study and is maintained at $90 microns$ to match the NASA prototype micro-nozzle described in Hitt et al.[7] The GAMBIT2.1 grid generation software (Fluent Inc.) was used to develop the two-dimensional computational meshes. Depending on the spike length, the grid size contained between $180,000$ and $250,000$ elements. The meshes have been refined to the point where simulations are independent of further grid refinement.

Governing Equations. Continuum modeling is assumed in this study; this can be justified *a posteriori* by performing a Knudsen number analysis of the computed flow field in the regions of interest. We note in passing that portions of the supersonic plume downstream of the spike will certainly be rarefied (non-continuum) and the model accuracy is degraded; however, these areas are sufficiently removed from the spike region such that thrust prediction is not compromised. The micronozzle flow field is thus governed by the compressible Navier-Stokes Equations which are solved using a coupled implicit solver for all simulations. The governing conservation

equations for mass, momentum, and energy are given by

$$\frac{\partial \rho}{\partial t} + \boldsymbol{\nabla} \cdot (\rho \mathbf{V}) = 0 \tag{4}$$

$$\frac{\partial}{\partial t}(\rho \mathbf{V}) + \boldsymbol{\nabla} \cdot (\rho \mathbf{V}\mathbf{V}) = -\boldsymbol{\nabla} p + \boldsymbol{\nabla} \cdot (\boldsymbol{\tau}) \tag{5}$$

$$\frac{\partial}{\partial t}(\rho E) + \boldsymbol{\nabla} \cdot (\mathbf{V}(\rho E + p)) = \boldsymbol{\nabla} \cdot (k \boldsymbol{\nabla} T + (\boldsymbol{\tau} \cdot \mathbf{V})) \tag{6}$$

$$E = h - \frac{p}{\rho} + \frac{\mathbf{V}^2}{2} \tag{7}$$

$$\boldsymbol{\tau} = \mu \left(\left(\boldsymbol{\nabla} \mathbf{V} + \boldsymbol{\nabla} \mathbf{V}^T \right) - \frac{2}{3} \boldsymbol{\nabla} \cdot \mathbf{V} \mathbf{I} \right). \tag{8}$$

In these equations, E is the specific energy, and p is the absolute local pressure, μ is the fluid viscosity, k is the thermal conductivity, T is the static temperature, h is the enthalpy, and $\boldsymbol{\tau}$ is the viscous stress tensor. The system is closed by the ideal gas law equation of state

$$p = \rho R T \tag{9}$$

No slip boundary conditions are imposed on the nozzle walls. Subsonic portions of the outlet boundaries are prescribed a constant back-pressure value of p_∞=1.0 kPa. This value serves to maintain the Knudsen number within the continuum regime for the aerospike region. For supersonic portions of the domain outlet, the pressure and all other flow quantities are extrapolated from the interior flow via the method of characteristics (Riemann invariants). A prescribed pressure is imposed at the inlet boundary, which is regarded as a stagnation value. Inlet gas properties are determined at the fully decomposed adiabatic flame temperature of 85% pure hydrogen peroxide, 886 K. Varying the pressure inlet boundary condition allows performance to be investigated at different throat Reynolds numbers (mass flow rates). In these simulations, the inlet pressure was varied from $p_0 = 25$ kPa to $p_0 = 250$ kPa results in a throat Reynolds number in the range of 60 to 830 and nozzle pressure ratios p_0/p_∞ ranging from 25:1 to 250:1.

The compressible Navier-Stokes equations were solved using the coupled implicit solver within the FLUENT6.2 software package. The first phase of iterations is done in the first-order descretization scheme, once the first-order convergence is determined, second order descretization schemes are implemented for the final solution convergence. The convergence of solution is determined by residuals and flow monitors established at key locations within the domain. The controlling flow monitors were placed at the locations where high pressure temperature and velocity gradients were identified. Conservation of mass through the nozzle was also carefully monitored and verified.

B. Rarefied Flow Modeling via DSMC

To provide an independent comparison to the continuum-based model predictions, rarefied flow calculations were also performed. Aside from simple validation, these calculations were intended to quantify the degree to which non-continuum effects contribute to predictions for thrust output. The direct simulation Monte Carlo (DSMC) code SMILE[10] was used to simulate aerospike nozzle expansion into vacuum. The hydrogen peroxide was modeled using the variable hard sphere model with the molecular diameter $d = 4.17 \times 10^{-10}$ m, viscosity-temperature exponent $\alpha = 0.31$ and the Larsen-Borgnakke model for internal energy relaxation with collisional numbers $Z_r = 5$ and $Z_v = 50$. The SMILE code uses two-level rectangular cells with automatic grid adaptation. The background collision cell size was $10\mu m$ with a maximum cell partition level of 10. The inflow boundary for the DSMC calculations was located at the aerospike nozzle exit and the exit velocity, temperature and pressure were based on the Navier-Stokes solution described above. For the case of vacuum expansion at inlet pressure of 25kPa, the total number of simulated molecules was about two million and the calculations took four hours using eight AMD Opteron 885 processors.

III. Numerical Results

Steady-state flows have been computed for full and truncated spikes for Reynolds numbers ranging from 64-830; plots showing Mach contours and streamline patterns appear in Figure 3. Overall, the flow behavior on

P inlet	100%Inv.	100%Vis.	40% Inv.	40%Vis.	20% Inv.	20%Vis.	DSMC 100%
250	31.7	29.7	30.1	24.2	27.2	23.9	28.1
200	26.9	22.7	23.9	21.3	21.7	18.9	-
150	19.8	16.8	18.1	15.5	17.1	13.9	-
100	13.5	12.0	11.8	10.0	10.8	9.0	-
75	10.1	9.0	9.0	7.5	8.2	6.5	-
50	7.6	4.9	6.0	4.5	5.4	4.1	-
25	4.0	2.4	3.0	1.9	2.8	1.8	1.93

Table 1. A summary viscous, quasi-inviscid and DSMC thrust values for the full aerospike and two truncated nozzles (20%, 40%). The pressure inlet values are in kPa and the thrust values are in μN per unit depth. The backpressure in all continuum cases is 1.0 kPa, and the backpressure for the DSMC case is a virtual vacuum at ~ 0 kPa.

the micro-scale exhibits many of the same general features reported in the aerospace literature for large-scale aerospike nozzles.[11] As expected for a fixed geometry, the changing Reynolds number alters the free boundary reflection mechanism – and hence the plume characteristics – corresponding to the varying pressure ratios p_0/p_∞. For the truncated spikes one also expects (from inviscid theory) somewhat different plume characteristics at a fixed Re since the expansion ratio A/A^* varies with spike length. Viscous effects are clearly evidenced by the flow separation at the base of the truncated spikes. At low Reynolds numbers, a notable viscous subsonic boundary layer forms along the surface of the spike and grows in thickness with downstream distance. Similar phenomena has been observed on the expander walls of supersonic linear micronozzles. For sufficiently low Reynolds numbers the subsonic layer can become sufficiently 'thick' so as to retard flow in the vicinity of the spike, which is the downstream of the throat. Shown in Figures 4-5 are the computed subsonic layer thicknesses at three different Reynolds numbers for the full spike and 20% spike configurations. The significant extent of the subsonic region is quite evident at the lowest values of the Reynolds numbers.

Thrust production has been calculated for full and truncated (20%, 40%) aerospikes for the range of inlet pressures (i.e., Re) and the results are plotted in Figure 6. It is found that there is very little difference in the thrust production at the lowest inlet pressure levels. Differences appear at the higher inlet pressures and flow rates, with the maximum thrust being yielded by the full spike. The results for the higher flow rates can be understood in terms of the effective expansion ratio (A/A^*). The relatively poor performance of the full spike at the lowest flow rates can be attributed to the mergence of significant viscous losses. Detailed examination of the flow field shows that the end result depends jointly on the viscous subsonic layer size and subsonic flow turning at the ends of the truncated spike.

Tabulated values of calculated thrust is compared with estimates obtained from quasi-inviscid simulations for different nozzle configurations and inlet pressures in Table 1. The degradation in performance arising from viscous effects is quite evident in this data. Of particular note is the relatively poor performance of the truncated aerospikes. On the macro-scale, this is a practical design consideration in which substantial weight savings can be obtained with modest reductions in thrust production, as evidenced by the inviscid results here. However, on the micro-scale, the flow separation effects at the lower Reynolds numbers result in much more severe penalties in performance – moreover, the savings in weight associated with a full aerospike is virtually negligible for a MEMS device. Thus, from a design perspective, it appears that only full (or nearly so) aerospike configurations should be considered.

Comparison with Rarefied Predictions. To assess the significance non-continuum flow effects, a limited number of comparisons of thrust predictions have been made with those obtained by DSMC calculations. Figure 7 shows a comparison of the continuum and DSMC density fields in the region of the full spike for a pressure inlet of 25 kPa. In general, the flow behavior is quite similar. The thrust results for the full spike at the two extreme inlet pressures of 25 kPa and 250 kPa appear in Table 1. It should be noted when making this comparison that the DSMC calculations were performed with a vacuum backpressure condition rather than 1 kPa owing to boundary condition constraints associated with the numerical algorithm. It is seen that at the highest flow rate the continuum and DSMC results differ by approximately 5% whereas almost a 25% difference is found

at the lowest flow rates. Some degree of discrepancy is expected owing to the different backpressure conditions in the continuum and DSMC calculations; with this in mind, the higher pressure inlet data are comparable. The significant discrepancy found at the low pressure inlet (low Re) case is a direct result of the greater subsonic region present and the different ambient backpressures are able to manifest themselves more strongly in the spike region of the flow. In summary, the studies so far suggest that continuum modeling is capable of capturing the necessary flow characteristics for thrust calculations.

Aerospike Efficiency. From a design perspective, it is useful to summarize the results obtained in terms of a nozzle efficiency. A common measure of the nozzle design efficiency is the normalized specific impulse I_{sp}^{*} defined by

$$I_{sp}^{*} \equiv \frac{I_{sp}}{I_{sp}^{opt}} \tag{10}$$

where

$$I_{sp}^{opt} \equiv \dot{m} g_0 \sqrt{\frac{2\gamma R T_0}{g_0^2(\gamma-1)}\left[1-\left(\frac{p_{exit}}{p_0}\right)^{\frac{\gamma}{\gamma-1}}\right]} \tag{11}$$

is the corresponding quasi 1-D theoretical value of the specific impulse. A plot of the aerospike efficiencies for different configurations at different Reynolds numbers appears in Figure 8. Here the relative inefficiency of the truncated spikes is quite apparent. The explanation for the weak, local maximum in efficiency for the full spike at $Re \sim 150$ is not immediately clear; however, such behavior has been observed for linear nozzles on the micro-scale.[12] To reiterate a previous point, unlike macro-scale aerospike designs where thrust-to-weight ratio is a key factor, micro-scale aerospike design can be based effectively on performance. Therefore the use of full-length spikes should be the target design, in as much as microfabrication techniques permit. While fully 3-D simulations are still needed for the linear aerospike, due to its geometry and "free boundaries" at the top and bottom vs. a fully enclosed structure for the linear nozzle, the 3-D effects are unlikely to incur the level of losses seen with the linear micro-nozzle. The truncated aerospike nozzles significantly reduce efficiency suggesting that such configurations may not be well suited for micro-scale nozzle design.

IV. Conclusions

In this paper we have presented the key results of a numerical investigation of linear aerospike nozzle performance on the micro-scale. To the best of our knowledge, this represents the first detailed analysis of this phenomena in the aerospace literature. The *ansatz* for examining a linear aerospike configuration for a micro-scale design is derived from its potential to allay viscous losses known to occur for internal micro-nozzle flows with multiple solid boundaries. It is observed that substantial subsonic layers form on the spike surface at low Re which degrade thrust production and efficiency by retarding the bulk flow. The efficiency (I_{sp}^{*}) of the 2-D full-length spike is found to be rather similar to 2D linear micronozzle findings that have been reported in the literature; however, the truncated versions of the spike can substantially *underperform* by comparison. With weight considerations negligible for micro-scale spikes, there seems to be little justification for consideration of plug nozzle configurations for MEMS-based devices.

This work has been limited to a 2-D flow model of the device operation, which does not capture the true 3-D nature of an actual MEMS nozzle which will necessarily have finite depth. We posit that a higher efficiency in 3-D will be realized over linear micro-nozzles since the linear aerospike will not have the *additional solid boundaries* and associated viscous losses. Indeed, our recent simulations of 3-D linear micro-nozzles have shown a 10-20% decrease in efficiency in comparison to the corresponding 2-D models linked to the two additional viscous subsonic layers.[13] We do not expect this degree of drop-off in performance for the aerospike. This is an area we are currently working on and expect to report our findings in the near future.

Acknowledgments

This work was supported by the United States Air Force Office of Sponsored Research (AFOSR) under Grants #FA49620-02-1-0230 and #FA9550-06-1-0364

References

[1]R.L. Bayt, and K.S. Breuer 1998 "Viscous Effects in Supersonic MEMS-based Micronozzles" Proc. 3rd ASME Microfluids Symp. (Anaheim, CA).

[2]R.L. Bayt, and K.S. Breuer, "System design and performance of hot and cold supersonic microjets," AIAA Paper 2001-0721, 2001.

[3]Alexeenko A A, Levin D A, Gimelshein S F, Collins R J, and Reed B D 2001 "Numerical Modeling of Axisymmetric and Three-Dimensional Flows in Microelectromechanical Systems Nozzles" AIAA Journal 40 897-904.

[4]Alexeenko AA and Levin D., ÒNumerical Simulation of High-Temperature Gas Flows in a Millimeter-ScaleThruster,Ó J. Thermophysics and HeatTransfer, 16 (1), 2002.

[5]Alexeenko, A.A., Levin, D.A., Fedosov, D.A., and Gimelshein, S.F., "Performance Analysis of Microthrusters Based on Coupled Thermal-Fluid Modeling and Simulation" J. of Propulsion and Power. Vol. 21, No. 1 2005.

[6]Louisos W.F. and Hitt D.L., "Supersonic Miconozzles," *Encyclopedia of Microfluidics & Nanofluidics*, in press.

[7]D.L. Hitt, C. Zakrzwski and M. Thomas, "MEMS-Based Satellite Micropropulsion Via Catalyzed Hydrogen Peroxide Decomposition," J. Smart Mater & Struct., Volume 10, pp. 1163-1175, 2001.

[8]Anderson, John D. Jr. "Modern Compressible Flow with Historical Perspective" McGraw-Hill Companies, Boston, MA, 2003.

[9]G. Angelino, "Approximate Method for Plug Nozzle Design" AIAA Journal, Vol. 2 (10), p. 3, 1964.

[10]M. S. Ivanov, G. N. Markelov and S. F. Gimelshein, "Statistical Simulation of Reactive Rarefied Flows: Numerical Approach and Applications, " AIAA Paper 98-2669.

[11]Ito T.,Fujii K., and Hayashi A. K., "Computations of Axisymmetric Plug Nozzle Flow Fields," AIAA Paper 99-3211.

[12]Louisos W.F., Alexeenko A.A., Hitt D.L. and Zilić A., "Design Considerations for Supersonic Micronozzles," Intl. J. Manufacturing Res., (in press).

[13]Louisos W.F. and Hitt, D.L., "Heat Transfer and Viscous Effects in 2D & 3D Micro-Nozzles," AIAA Paper 2007-3987.

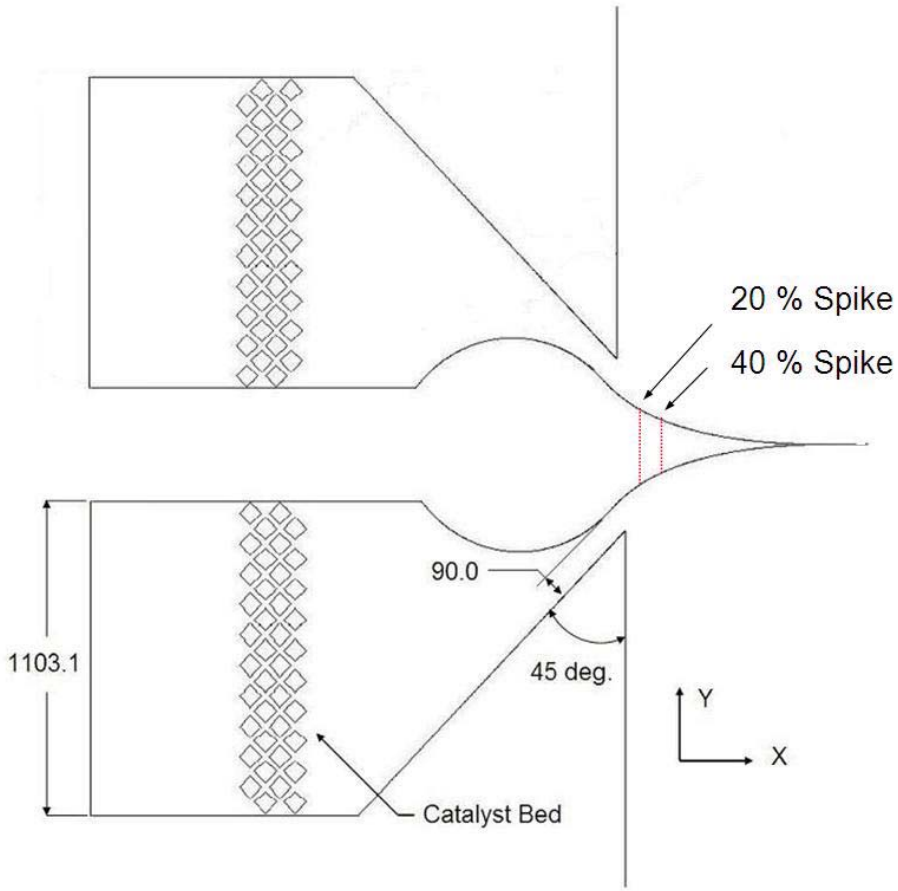

Figure 1. Geometry of the monopropellant linear aerospike supersonic micro-nozzle including a 20% and 40% truncation locations as shown. Note the base formation once the nozzle in truncated. All units are in microns.

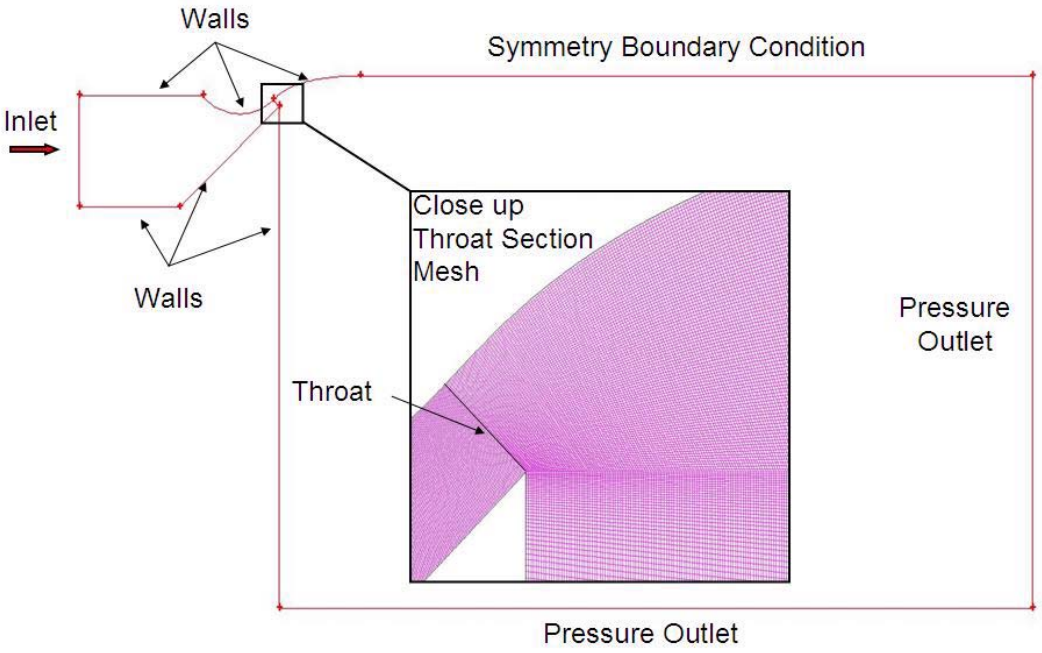

Figure 2. The 2-D computational domain including the boundary conditions for the nozzle flow problem. The symmetry condition was employed to decrease computational expense.

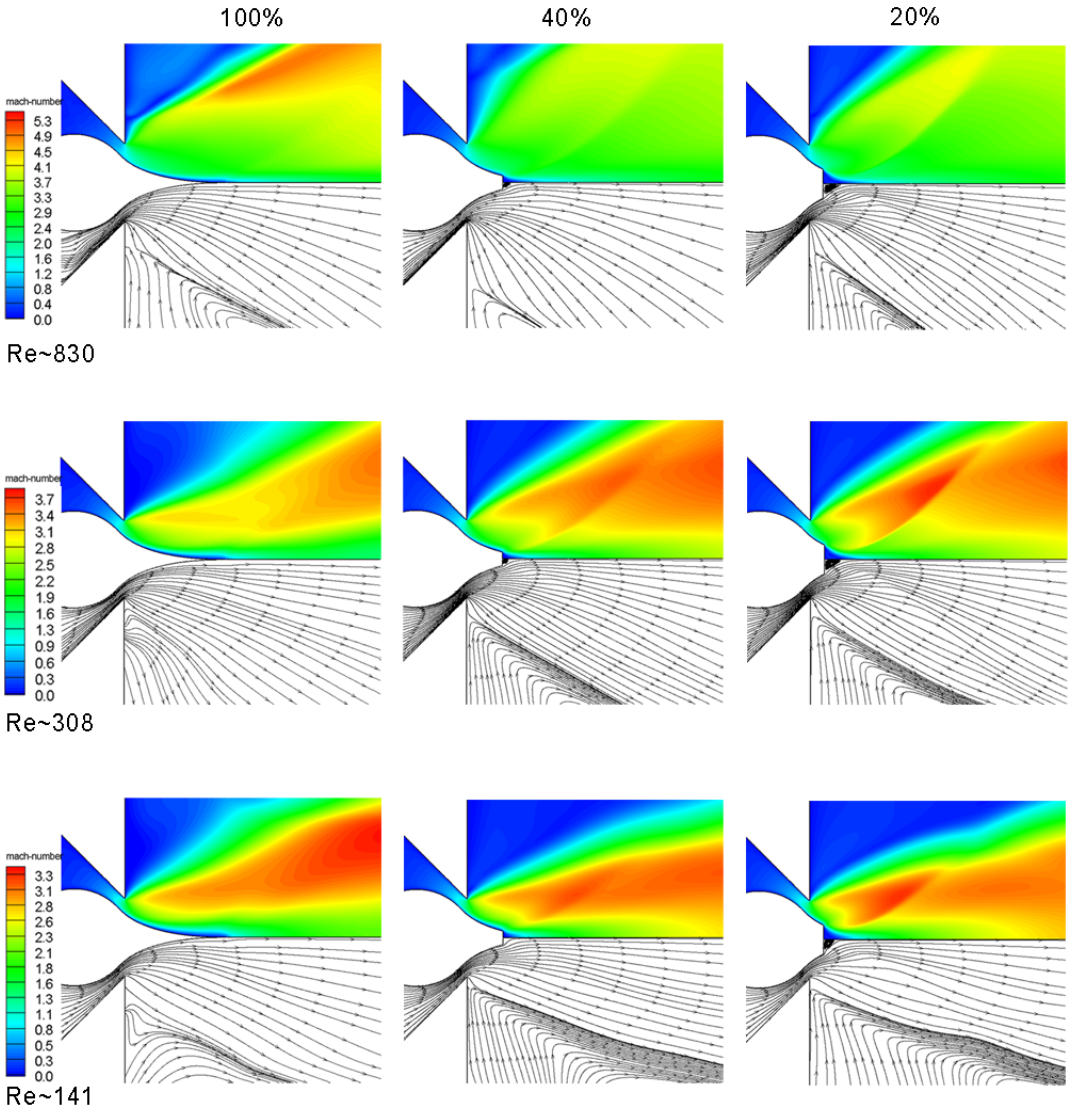

Figure 3. Mach number contours and streamlines for different spike configurations, Reynolds numbers and fixed backpressure of $1kPa$.

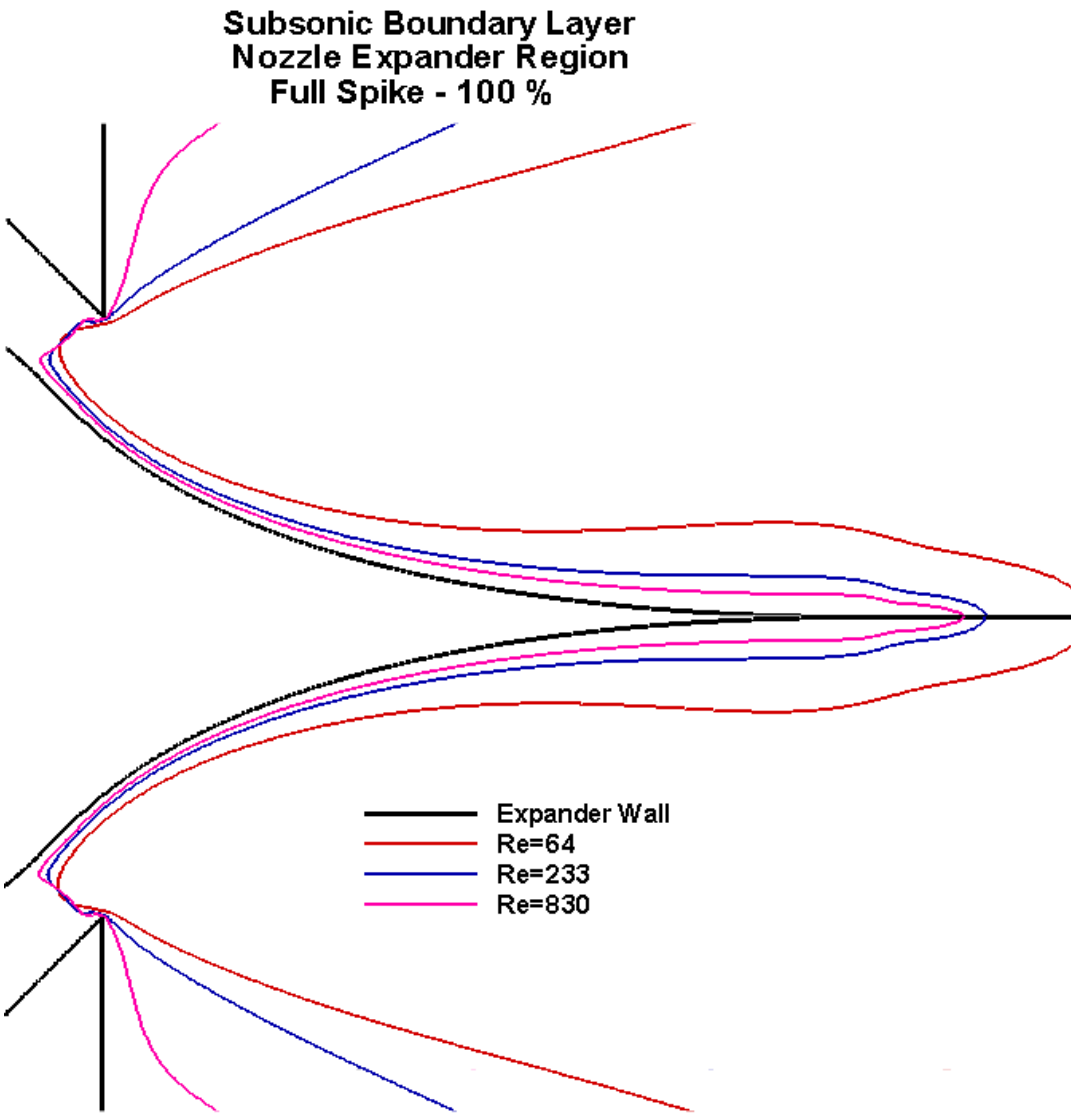

Figure 4. Subsonic layer boundaries for the *full* spike for different Reynolds numbers.

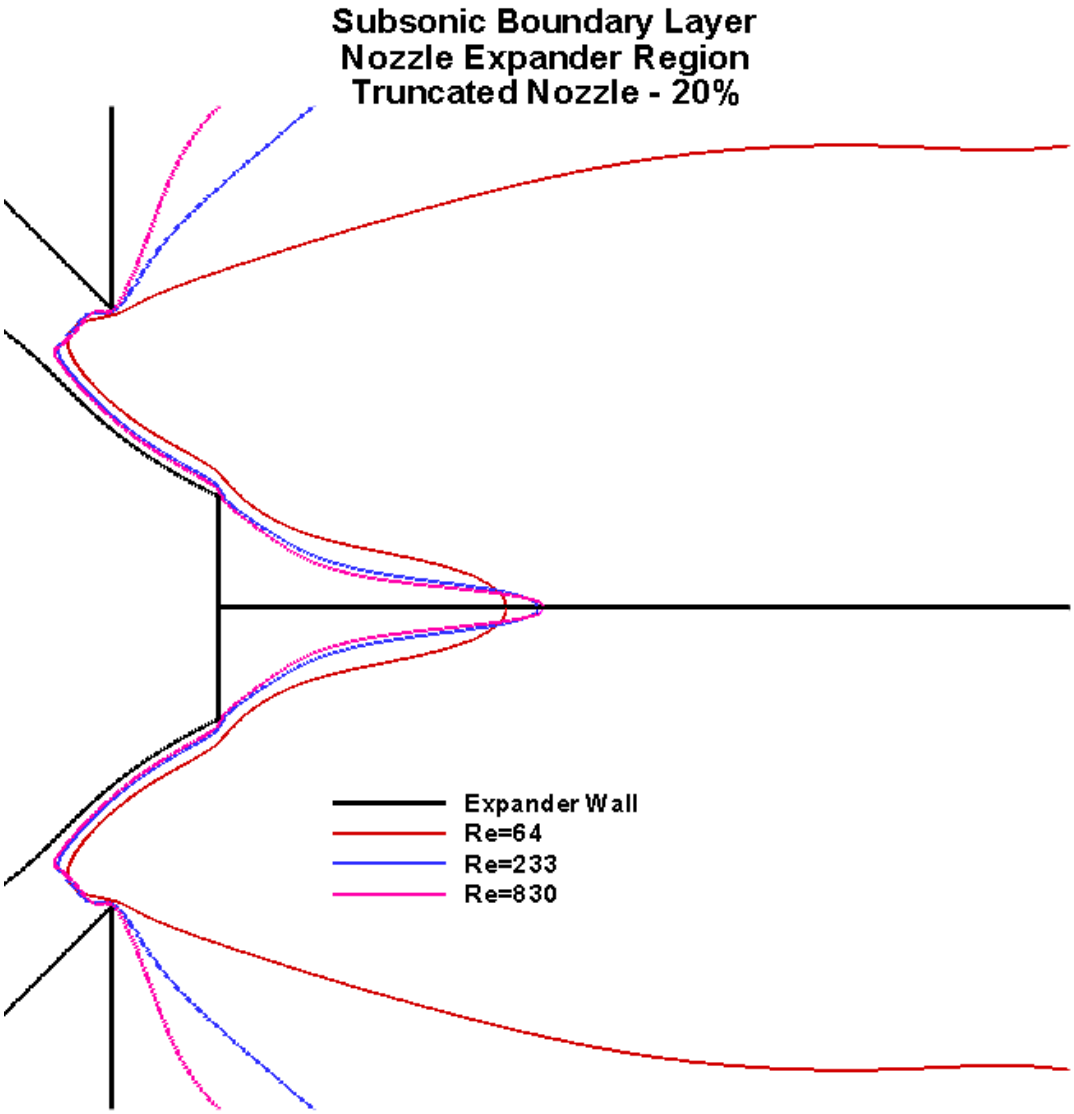

Figure 5. Subsonic layer boundaries for the *truncated* (20%) spike for different Reynolds numbers.

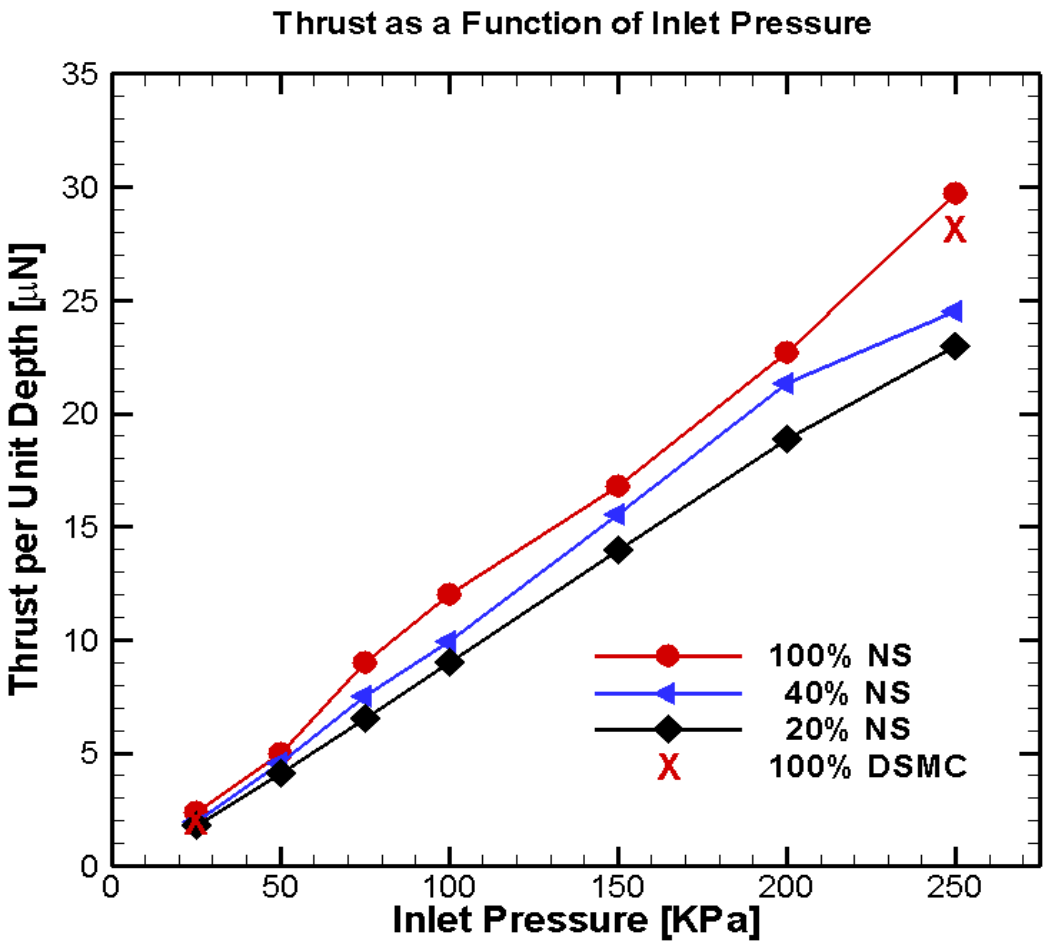

Figure 6. Plot of viscous thrust in micro-Newtons per unit depth as a function of nozzle inlet pressure.

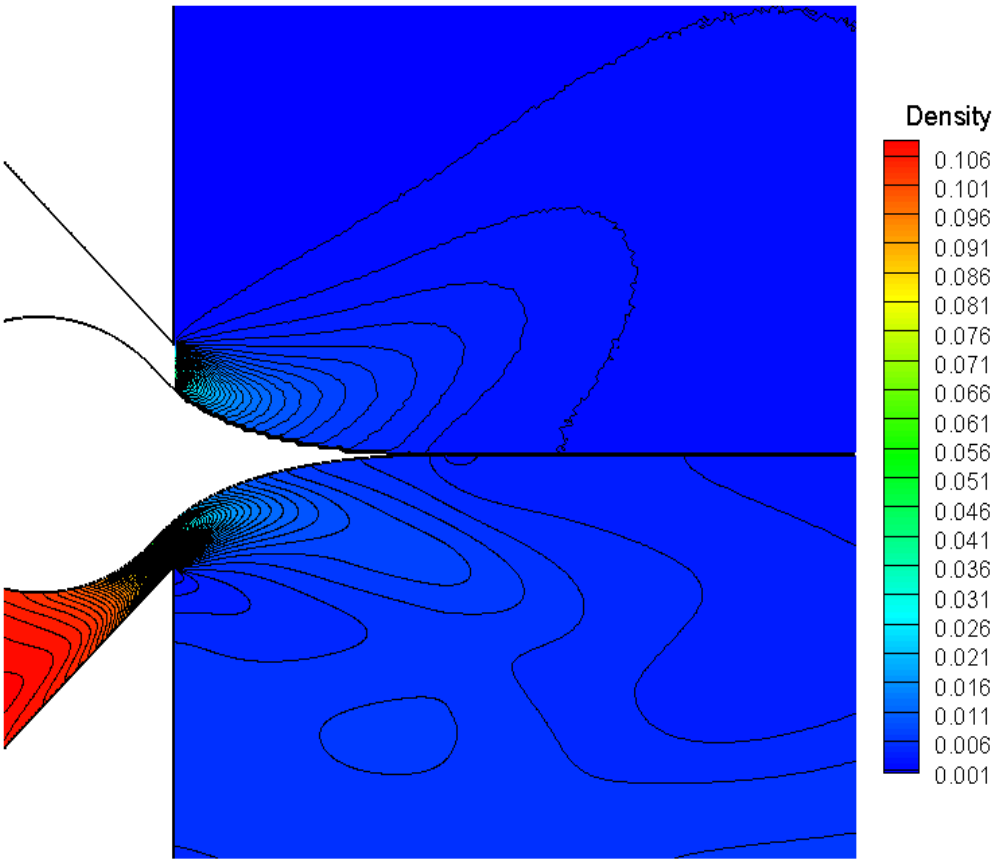

Figure 7. Plot showing a comparison of the continuum (bottom half) and DSMC (top half) density field in the $full$ spike region for a pressure inlet of $25kPa$. DSMC calculations were performed with a vacuum back pressure while continuum approach used $1.0kPa$ back pressure.

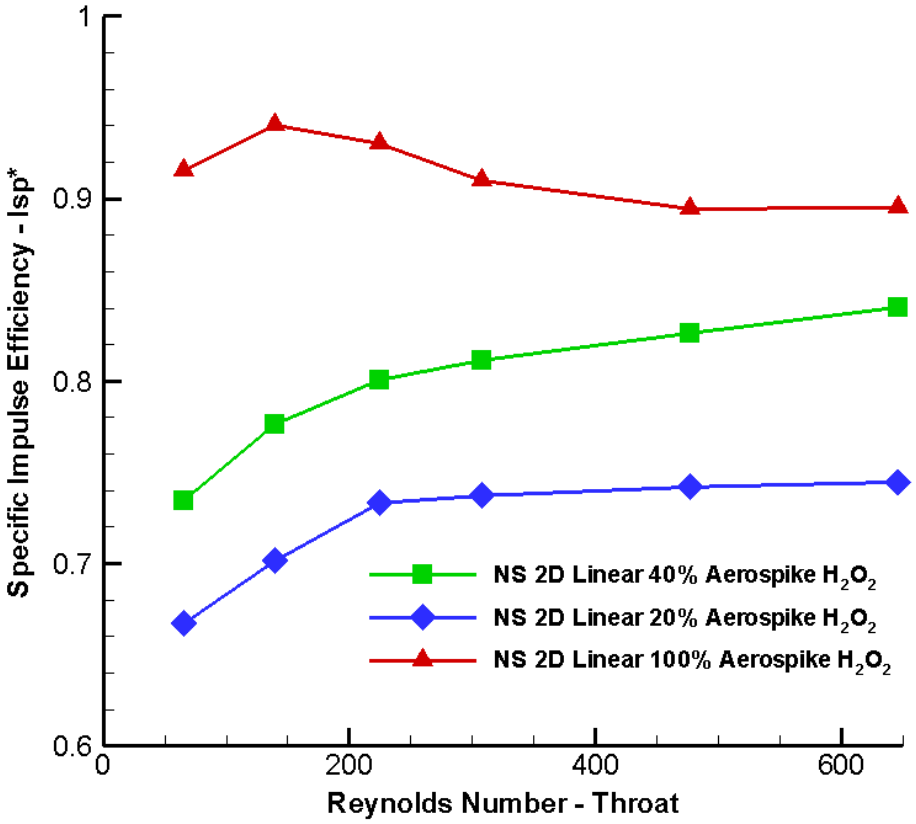

Figure 8. A summary plot of linear aerospike micro-nozzle efficiencies I_{sp}^{*} for various nozzle configurations as a function of the throat Reynolds number.